LOW-SPEED FLOWS INVOLVING BUBBLE SEPARATIONS

ITIRO TANI

Aeronautical Research Institute, University of Tokyo

LIST OF SYMBOLS

a ratio of velocity on boundary streamline to that at outside of boundary layer or entrainment region
c aerofoil chord
C_L lift coefficient of aerofoil section
C_p pressure coefficient defined by $(p - p_0)/\frac{1}{2}\varrho\, U_0^2$
d diameter of circular cylinder
H ratio of displacement and momentum thicknesses of boundary layer
h height of bubble
l length of bubble defined by the distance from separation to reattachment, $l_1 + l_2$
l_1 distance from separation to transition
l_2 distance from transition to reattachment
p pressure
p_0 free-stream pressure
p_r pressure at reattachment
p_s pressure at separation
p_t pressure at transition
R Reynolds number based on free-stream velocity and aerofoil chord or cylinder diameter, $U_0\, c/\nu$ or $U_0\, d/\nu$
$R_{\delta_s^*}$ boundary-layer Reynolds number based on displacement thickness at separation, $U_s\, \delta_s^*/\nu$
s distance along upper surface of aerofoil from leading edge
s' distance along surface from stagnation point
U velocity outside of boundary layer
U_0 free-stream velocity
$U_{\max}$ peak value of velocity outside of boundary layer
U_r velocity outside of boundary layer at reattachment
U_s velocity outside of boundary layer at separation
U_t velocity outside of boundary layer at transition
u velocity within boundary layer
x distance along aerofoil chord from leading edge

y distance normal to aerofoil surface
α incidence of aerofoil section, uncorrected for tunnel-wall constraint
δ_r boundary-layer thickness at reattachment
δ_t distance between bubble top and edge of boundary layer
δ_s^* boundary-layer displacement thickness at separation
θ_s boundary-layer momentum thickness at separation
φ angular distance from stagnation point
ν kinematic viscosity of fluid
ϱ density of fluid
σ pressure recovery coefficient defined by $(p_r - p_s)/\frac{1}{2}\varrho\, U_s^2$
τ average value of shear stress in turbulent entrainment

1. INTRODUCTION

Observations at low subsonic speeds have shown that when a laminar boundary layer separates from a surface the flow often becomes reattached to the surface some distance downstream as a turbulent boundary layer. The region underneath the separated flow, between the points of separation and reattachment, and set into circulatory motion, is commonly referred to as a *laminar separation bubble* or simply as a *bubble.*

The bubble is best known because of its occurrence on the upper surface of aerofoils at incidence. It plays an important part in determining the behaviour of the boundary layer on the surface, and consequently the stalling characteristics of aerofoils. However, the occurrence of the bubble is not necessarily confined to aerofoils. It is observed also on circular cylinders at Reynolds numbers within the critical range over which the drag coefficient experiences a considerable change. Another example is furnished by the interaction between an oblique shock wave and a laminar boundary layer on a flat plate at supersonic speeds.

This paper presents a review of the published results on the flow involving separation bubbles. First, the experimental results on aerofoils that illustrate the formation of a separation bubble and its behaviour in relation to stalling characteristics are described. Further experimental results are presented to indicate the confinement of bubble formation to a certain range of Reynolds numbers. Some results for circular cylinders are also presented. The experimental data are then analysed in order to describe the formation and behaviour of a bubble in terms of a Reynolds number typical of local conditions in the boundary layer. Finally, a critical examination is made of various theories which have been postulated as to the mechanism of separation bubbles with a view to gaining a better understanding of the fundamental aspects of the phenomenon. Consideration is confined to two-dimensional flow at low subsonic speeds only.

The paper was prepared by revising and enlarging the author's review[41] on the subject published in 1961.

2. THREE TYPES OF STALL AND ASSOCIATED SEPARATED FLOWS

The classification of stalling characteristics of aerofoils dates back to Melvill Jones's investigation[4, 5] in the early nineteen-thirties. Jones classified stall into three basic types: a type of stall caused by flow separation near the trailing edge, and two types of stall caused by separation near the leading edge. However, direct correlation of the types of stall with boundary-layer characteristics was not possible until remarkably detailed mea-

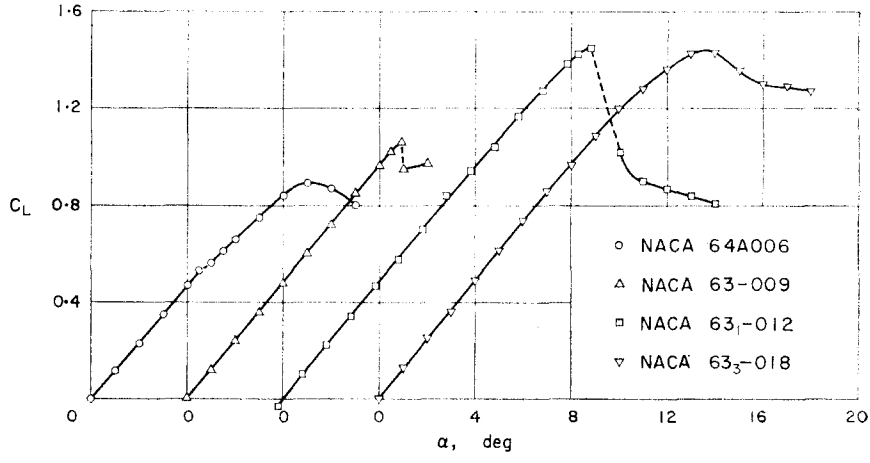

FIG. 1. Variation of section lift coefficient with incidence for NACA 64A006, 63-009, 63_1-012 and 63_3-018 aerofoil sections. $R = 5{\cdot}8 \times 10^6$. Measurements by McCullough and Gault.[22]

surements were made by McCullough and Gault[18, 19] in the late nineteen-forties.

According to McCullough and Gault[22], the three types are: *trailing-edge stall*, preceded by a movement of the separation point of the turbulent boundary layer forward from the trailing edge with increasing incidence; *leading-edge stall*, caused by an abrupt separation of the laminar boundary layer near the leading edge without subsequent reattachment; and *thin-aerofoil stall*, preceded by a laminar separation near the leading edge, with turbulent reattachment at a point which moves progressively rearward with increasing incidence. Typical examples of these types of stall are provided by the experimental data for the NACA 63_3-018, 63_1-012 and 64A006 aerofoil sections, obtained at a Reynolds number of $5{\cdot}8 \times 10^6$. As shown in Fig. 1, the lift variation with incidence† is gradual and continuous for the NACA 63_3-018 section, which experiences trailing-edge stall, while it shows an abrupt discontinuity at the stall for the NACA 63_1-012 section, which

† All the values of incidence referred to in the present paper are those uncorrected for the constraint of the tunnel walls.

undergoes leading-edge stall. The lift curve of the NACA 64A006 section, which experiences thin-aerofoil stall, is characterized by a rounded peak, preceded by a slight discontinuity at an incidence of 5°. Also shown in the figure is the lift curve of the NACA 63-009 section, which stalls in a manner similar to the NACA 63_1-012 section except that the lift discontinuity at the stall is less severe.

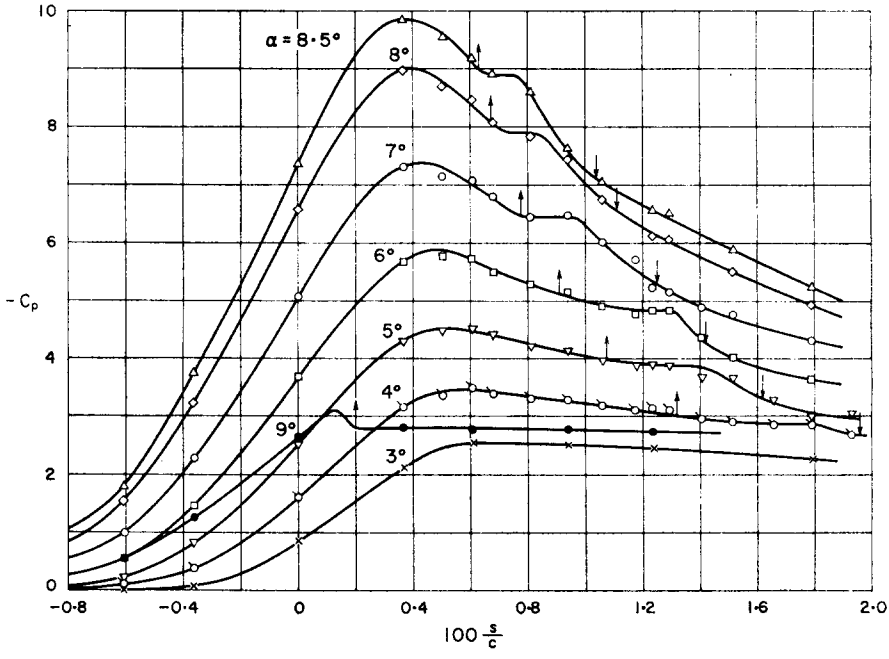

FIG. 2. Pressure distribution near the leading edge of NACA 63-009 aerofoil section at $R = 5{\cdot}8 \times 10^6$. Measurements by McCullough and Gault[18, 22].

Detailed observations[18, 22] by means of pressure distribution measurements and the liquid-film technique reveal that separation of the laminar boundary layer takes place prior to the stall near the leading edge of the NACA 63_1-012 and 63-009 sections, and that the separated flow reattaches to the surface within a short distance to form a separation bubble in the underlying region. The length or streamwise extent of the bubble is of the order of one per cent of the aerofoil chord, so that its presence has no significant effect on the pressure distribution except for the appearance of a minute bump.

Figure 2 shows the pressure distributions near the leading edge on the surface of the NACA 63-009 section[18, 22], values of the non-dimensional pressure coefficient $C_p = (p - p_0)/\frac{1}{2}\varrho\, U_0^2$ being plotted against the non-

dimensional distance s/c. Here p is the pressure on the surface, p_0 is the free-stream pressure, U_0 is the free-stream velocity, ϱ is the density, c is the chord, and s is the distance along the upper surface measured from the leading edge. The positions of separation and reattachment, as determined by the liquid-film method, are shown by the upward and downward arrows, respectively. A separation bubble is first discernible at an incidence of 4°,

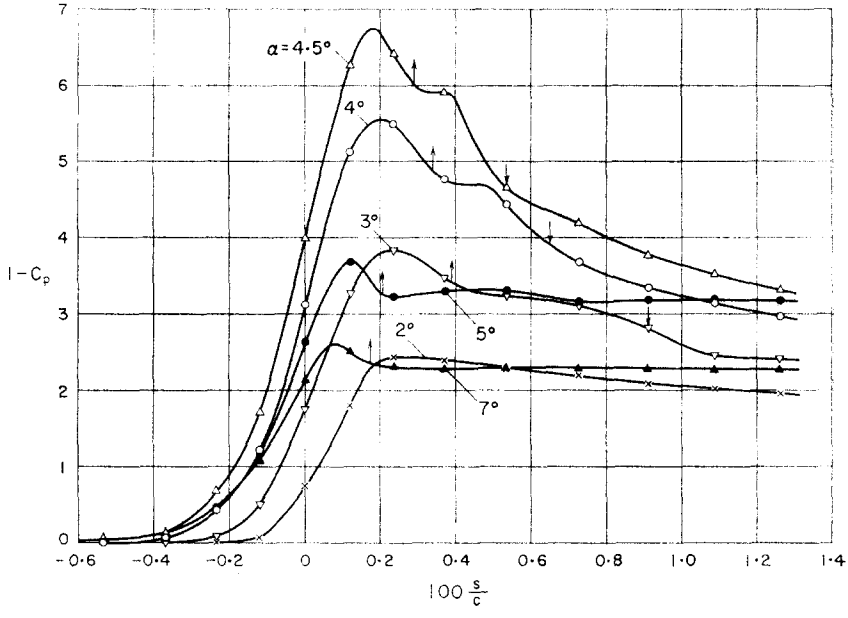

FIG. 3. Pressure distribution near the leading edge of NACA 64A006 aerofoil section at $R = 5{\cdot}8 \times 10^6$. Measurements by McCullough and Gault.[19,22]

and persists up to higher incidences. An increase in incidence causes the bubble to move forward and contract in streamwise extent. A small region of constant pressure exists within the bubble, although pressure recovery begins upstream of the point of reattachment. A further increase in incidence eventually moves the separation point so far forward that the flow no longer reattaches to the surface within a short distance. The bubble has then *broken down* or *burst*. This occurs at an incidence of 9°, and is accompanied by a redistribution of the pressure into the flattened form, and by an abrupt loss of lift. Maximum lift is attained at an incidence of 8·9°.

Figure 3 shows the pressure distributions near the leading edge of the NACA 64A006 section.[19,22] The presence of a separation bubble is revealed for incidences from 3° to 4·5°. At an incidence of 5°, the bubble breaks down, which causes the above-mentioned slight discontinuity in the

lift curve. However, the breakdown does not lead to a complete separation of the flow; instead, the separated flow passes above the aerofoil surface and reattaches farther downstream. This is seen from the pressure distributions for higher incidences shown in Fig. 4, in which the pressure coefficient C_p is plotted against the chordwise distance x/c, and the positions of reattachment, as determined from velocity-profile measurements, are indicated by arrows. With increasing incidence the reattachment point moves

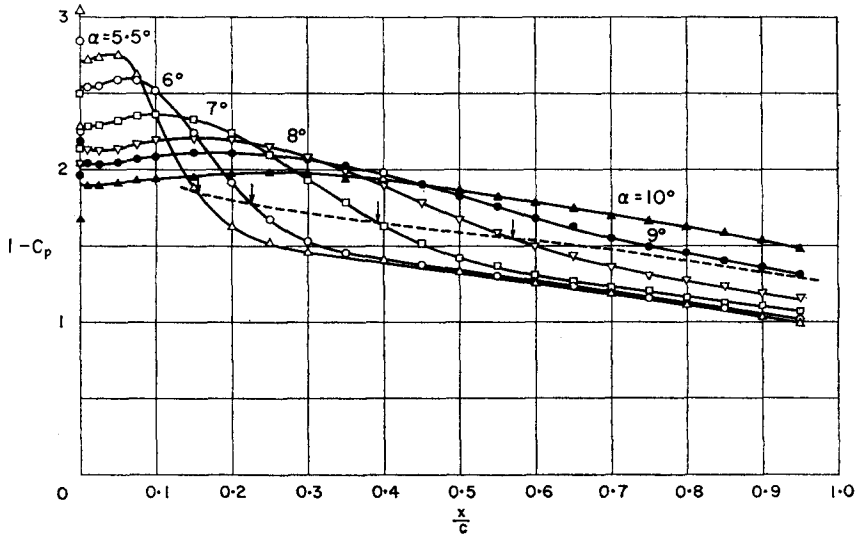

FIG. 4. Pressure distribution on NACA 64A006 aerofoil section for higher incidences at $R = 5{\cdot}8 \times 10^6$. Measurements by McCullough and Gault.[19, 22]

progressively rearward until it reaches the trailing edge for an incidence o about 9°, at which maximum lift is attained.

The region underneath the separated flow is formed of more or less quiescent or slowly circulating fluid, and is commonly referred to as a *dead-air region* or a *long bubble*. It has a length of several per cent of the aerofoil chord upon formation at low incidence, and grows rapidly with increasing incidence until it extends over the entire chord, at which stage its maximum thickness is about 3 per cent of the chord. It is considerably longer than the separation bubbles previously described, which occur on the NACA 64A006 section at incidences less than 5° and on the NACA 63-009 section at incidences less than 9°. For distinction these separation bubbles are termed *short*. It appears preferable, however, to distinguish the two types of bubble by their different effects on the pressure distribution, rather than by their different lengths. The presence of a long bubble makes the pressure distribution radically different from that in inviscid flow, with the

result that the sharp suction peak near the leading edge is not realized. Instead, a suction plateau of a reduced level extends over the region occupied by the bubble length. The suction plateau is lowered and lengthened by an increase of incidence. Conversely, the presence of a short bubble does not greatly affect the peak suction, which continues to increase as the incidence is increased up to the stall.

Figure 5 shows the pressure distributions for incidences just beyond the breakdown of a short bubble on the NACA 63-009 and 63_1-012 sections.[18, 22]

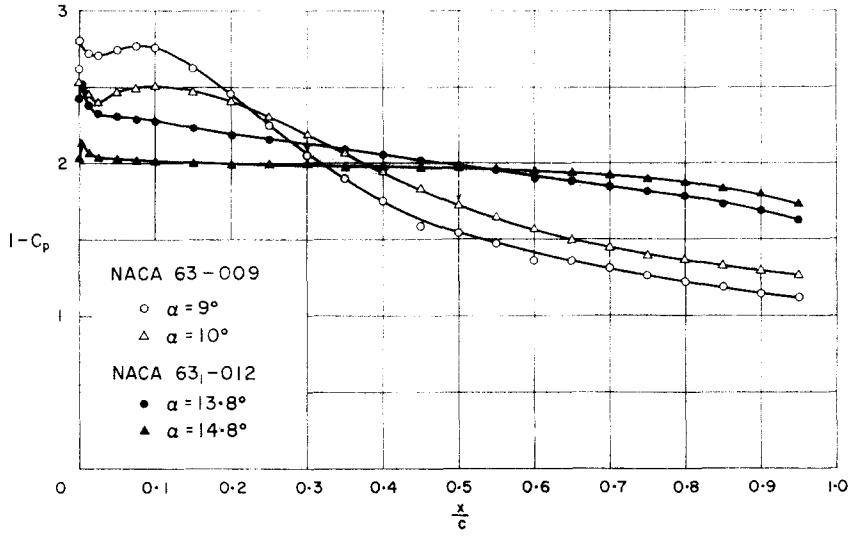

FIG. 5. Pressure distribution on NACA 63-009 and 63_1-012 aerofoil sections for incidences beyond the stall at $R = 5{\cdot}8 \times 10^6$ and $4{\cdot}1 \times 10^6$, respectively. Measurements by McCullough and Gault.[18, 22]

By comparison with the data of Fig. 4, the positions of reattachment are estimated to be those shown by arrows for the NACA 63-009 section, for which no measurements are reported. On the other hand, there is no evidence of reattachment on the NACA 63_1-012 section, and this accounts for the severe discontinuity of lift at the stall. It appears that up to the stall, the NACA 63-009 section exhibits the characteristics of the leading-edge stall, but after the stall assumes the type of flow that precedes the thin-aerofoil stall.

The characteristics of the NACA 64A006 section at a Reynolds number of $5{\cdot}8 \times 10^6$ provide an example in which the breakdown of a short bubble at an incidence of 5° gives rise to the formation of a long bubble. An increase in either the aerofoil thickness ratio or the Reynolds number increases the critical incidence until, for the thicker sections at least, maximum lift

is attained before the flow change occurs.[28] This observation affords a unified interpretation of leading-edge and thin-aerofoil stalls.

Finally, the formation of a short bubble is also detected at moderate incidences on thick aerofoils, such as the NACA 63_3-018 section, which experiences trailing-edge stall.[22] With increase in incidence, the bubble contracts but never breaks down before the attainment of maximum lift, which is determined by the forward movement of the separation point of the turbulent boundary layer. Here the role of the bubble is to make the boundary layer turbulent and affect the stalling characteristics through the initial thickness of the turbulent boundary layer.[14]

It should be noted that the examples given in this section are based on data obtained at a Reynolds number of $5{\cdot}8 \times 10^6$. A change in Reynolds number will undoubtedly affect the stalling characteristics, and may cause the stall of a given aerofoil section to change from one classification to another.

3. EFFECTS OF REYNOLDS NUMBER ON BUBBLE SEPARATION

It seems advisable at this stage to consider briefly the conditions under which the formation of a short bubble is possible. An obvious condition is the existence of an adverse pressure gradient steep enough to cause laminar separation. But this does not necessarily mean that a bubble will actually be formed. If the Reynolds number is sufficiently high, transition from laminar to turbulent flow will take place ahead of the "theoretical laminar separation point", namely that point at which separation would have occurred if the boundary layer had remained laminar. Under these circumstances, the bubble formation will be precluded. On the other hand, if the Reynolds number is sufficiently low, the separated flow will not reattach to the surface and no bubble will be formed. It appears, therefore, that the bubble formation is possible only for a certain range of Reynolds numbers, which will depend on the pressure distribution, the surface curvature, the surface roughness, and the turbulence of the free stream. In this section some examples are presented to illustrate the effect of Reynolds number on bubble separation.

At low Reynolds numbers the aerodynamic characteristics of aerofoils are rather poor because of laminar separation without subsequent reattachment. A typical example is provided by Kraemer's[38] measurements of the pressure distribution on the Göttingen 801 aerofoil section (Fig. 6). The estimated positions of separation and reattachment are shown in the figure by arrows. At a Reynolds number of $4{\cdot}2 \times 10^4$, the pressure distributions are relatively flat along the entire chord, characteristic of most separated flows. At a Reynolds number of $7{\cdot}5 \times 10^4$, however, the pressure distributions exhibiting a flat portion are indicative of the presence of a separation bubble. The bubble is not as short in extent as those observed

at higher Reynolds numbers (Figs. 2 and 3), but it should still be termed short in that the peak suction is attained near the leading edge. Figures 7 and 8 show the flow patterns about the same aerofoil obtained in a smoke tunnel at two Reynolds numbers.† The contrast between the two flow patterns is consistent with that shown by the pressure distribution data.

The results just discussed indicate that there exists a critical value of Reynolds number below which bubble formation is not possible, so that

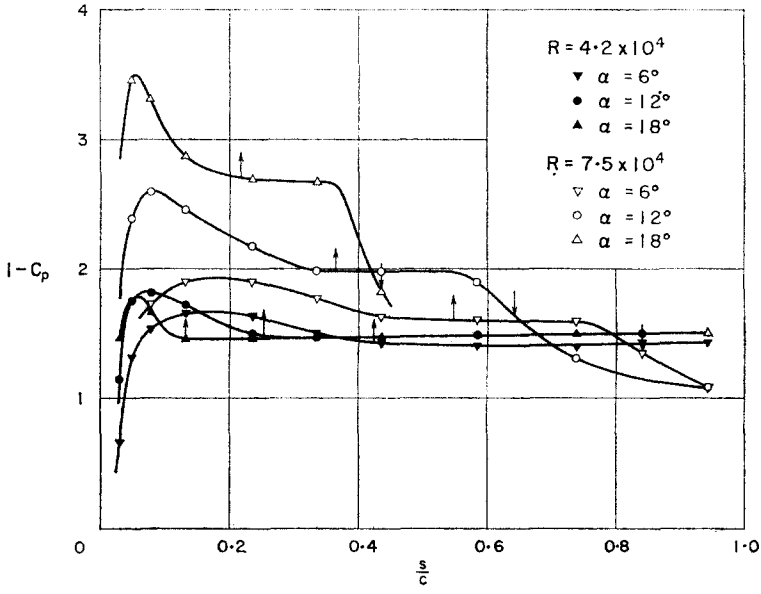

FIG. 6. Pressure distribution on Göttingen 801 aerofoil section at $R = 4{\cdot}2 \times 10^4$ and $7{\cdot}5 \times 10^4$. Measurements by Kraemer.[38]

the lift is low and the drag is high (subcritical state). At supercritical Reynolds numbers a bubble is formed, resulting in high lift and low drag. From force measurements made on the same aerofoil[38], the critical Reynolds number is believed to be about 6×10^4, but this value is valid only for the particular aerofoil. It seems preferable to correlate the critical change with a Reynolds number typical of local conditions in the boundary layer. This will be discussed in Section 5.

As the next example, Fig. 9 shows Gault's[27] experimental pressure distributions near the leading edge of the NACA 66_3-018 aerofoil at three values of Reynolds number and at an incidence of 15°, which corresponds approximately to the incidence for maximum lift. The positions of separation and reattachment, as determined by the liquid-film method, are shown

† The author is indebted to Professor H. Nakaguchi for taking pictures in the smoke tunnel at the Department of Aeronautics, University of Tokyo.

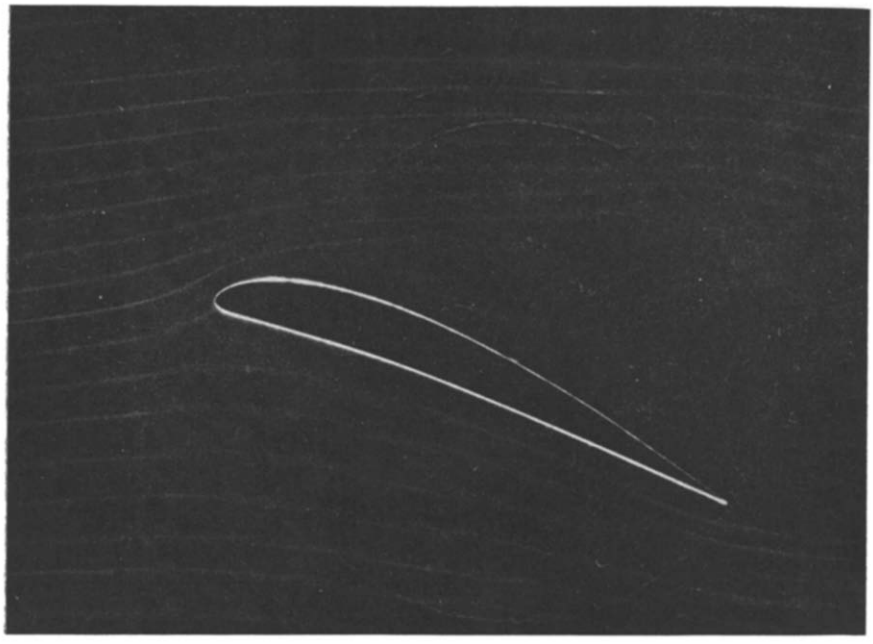

FIG. 7. Flow about Göttingen 801 aerofoil at a subcritical Reynolds number showing laminar separation without reattachment.

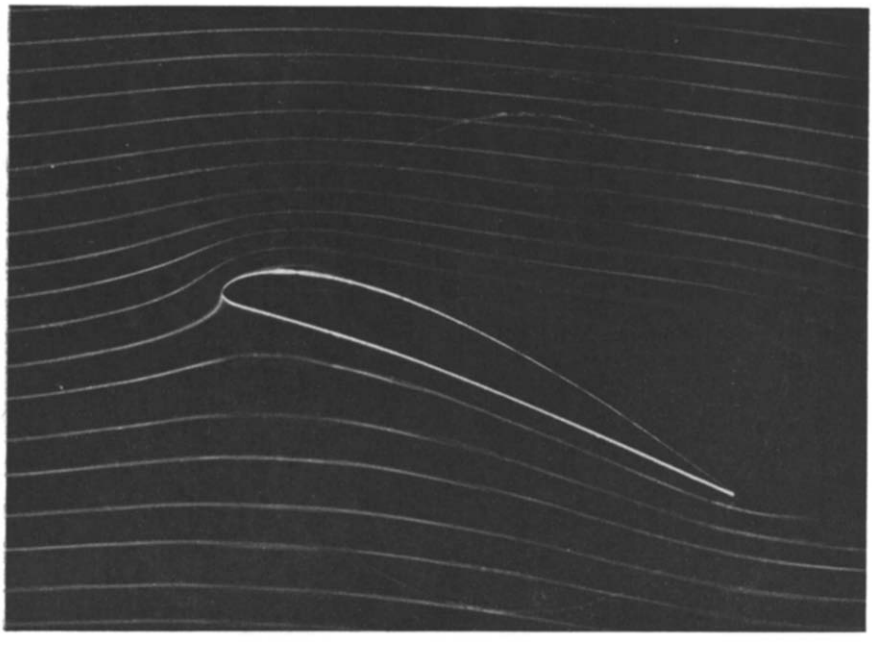

FIG. 8. Flow about Göttingen 801 aerofoil at a supercritical Reynolds number showing laminar separation followed by reattachment.

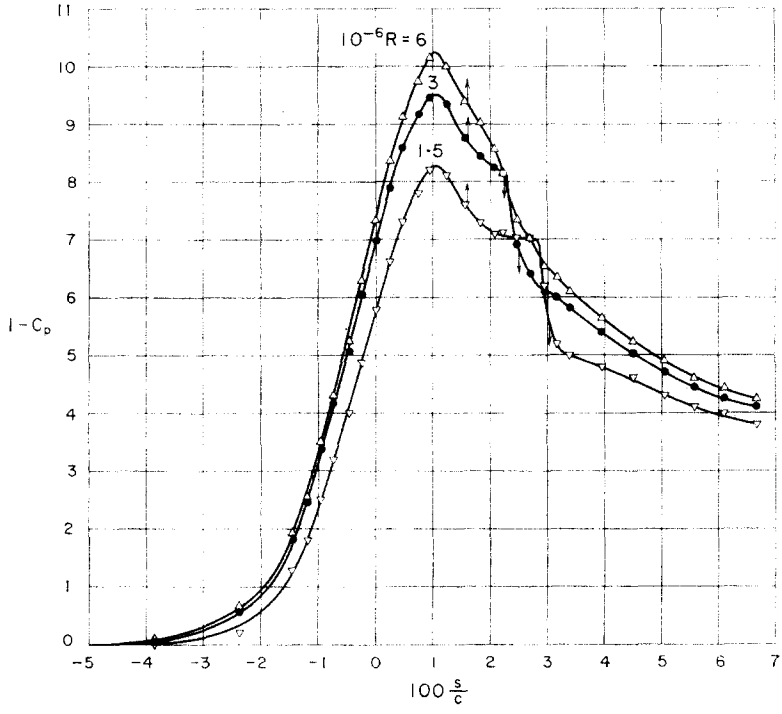

FIG. 9. Pressure distribution near the leading edge of NACA 66_3-018 aerofoil section at $\alpha = 15°$. Measurements by Gault.[27]

by upward and downward arrows, respectively. At Reynolds numbers less than about 4×10^6 the stall is abrupt (leading-edge stall), and is accompanied by a laminar separation without subsequent reattachment. The stall becomes more gradual as the Reynolds number is increased beyond 4×10^6. Coincident with this change, the length of the bubble is shortened by the increase in Reynolds number. It should also be noted that the presence of a bubble is not necessarily accompanied by a region of relatively constant pressure. The regions of constant pressure observed in previous examples are not apparent in Fig. 9 except at the lowest Reynolds number.

As the third example, Fig. 10 shows the pressure distribution on the same aerofoil[27] at four values of Reynolds number and at an incidence of 2°, which corresponds approximately to the limit of the low-drag range. Inspection of the data indicates that at lower Reynolds numbers the laminar boundary layer separates behind the position of maximum suction and subsequently reattaches to the surface as a turbulent boundary layer. However, increasing the Reynolds number beyond about 6×10^6 obliterates evidence of laminar separation, which is considered to be precluded by

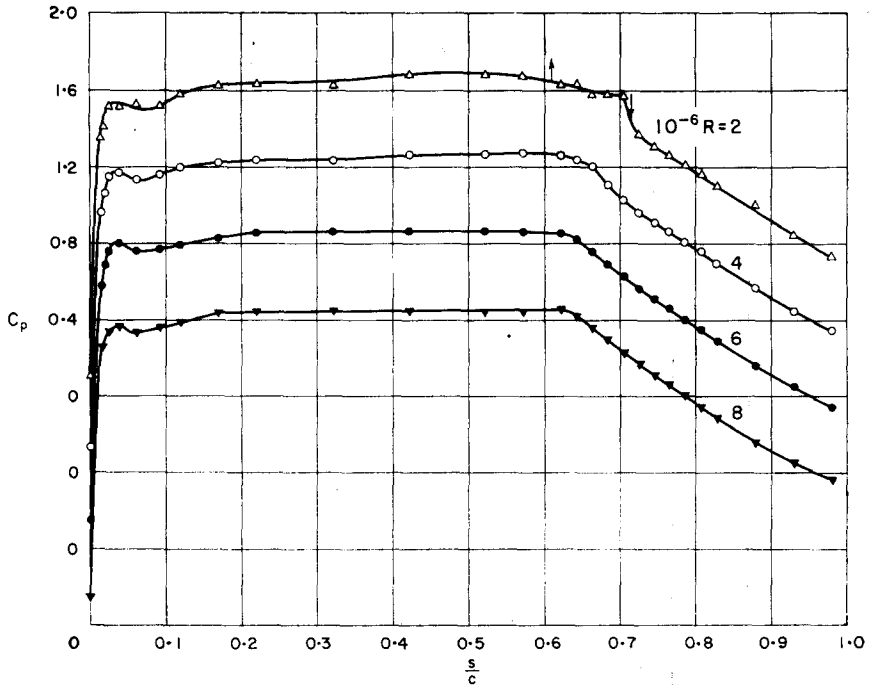

FIG. 10. Pressure distribution on NACA 66_3-018 aerofoil section at $\alpha = 2°$. Measurements by Gault[27].

transition to turbulence in the boundary layer. The bubble disappears in these circumstances. This effect will also be discussed in Section 5 in terms of a Reynolds number related to the boundary layer flow.

4. FLOW PAST A CIRCULAR CYLINDER INVOLVING BUBBLE SEPARATION

The examples presented so far have been confined to bubble separation on aerofoils. However, the occurrence and importance of the bubble are not necessarily confined to the flow past aerofoils. The presence of bubbles on circular cylinders and spheres manifests itself by the well-known change in flow pattern on passing through the critical range of Reynolds numbers. At subcritical Reynolds numbers the separation is laminar, but at supercritical Reynolds numbers there is a laminar separation bubble followed by reattachment as a turbulent boundary layer which subsequently separates, with the result that the wake is smaller, and the drag is reduced.

Figure 11 shows the pressure distributions on a circular cylinder at three Reynolds numbers in the critical range, taken from the classical measurements by Fage and Falkner.[3] The pressure coefficient C_p is plotted

against the angular distance φ from the stagnation point. The positions of separation estimated from the measurements of surface friction are indicated by arrows. It is seen that the bubble is present only at higher Reynolds numbers, and that the critical Reynolds number is between $1{\cdot}06 \times 10^5$ and $1{\cdot}66 \times 10^5$.

Also included in Fig. 11 is a result obtained in the disturbed stream behind a rope netting. The pressure distribution indicates the presence of a

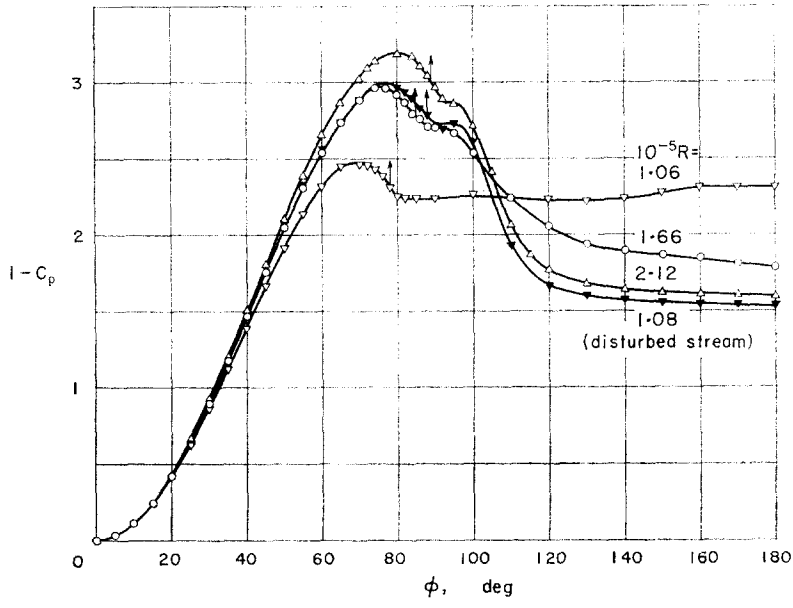

FIG. 11. Pressure distribution on circular cylinder. Measurements by Fage and Falkner[8]. Uncorrected for tunnel-wall constraint.

bubble even at a Reynolds number of $1{\cdot}08 \times 10^5$. This offers an example of an increase in free-stream turbulence reducing the critical Reynolds number.

Figure 12 shows a similar example for the pressure distribution on a circular cylinder mounted in a less turbulent stream, taken from the recent measurements by Yamamoto and Iuchi.[43] The positions of separation, transition and reattachment as indicated by a liquid issuing from a hole on the surface are shown by upward arrows, vertical marks and downward arrows, respectively. The change in Reynolds number is in sufficiently small steps to narrow the band of uncertainty of the critical Reynolds number. A remarkable feature is the rapid change, amounting practically to a discontinuity, from subcritical to supercritical pressure distribution. This is shown also by the curves of Fig. 13, in which the observed positions of separation, transition and reattachment are plotted against the Reynolds

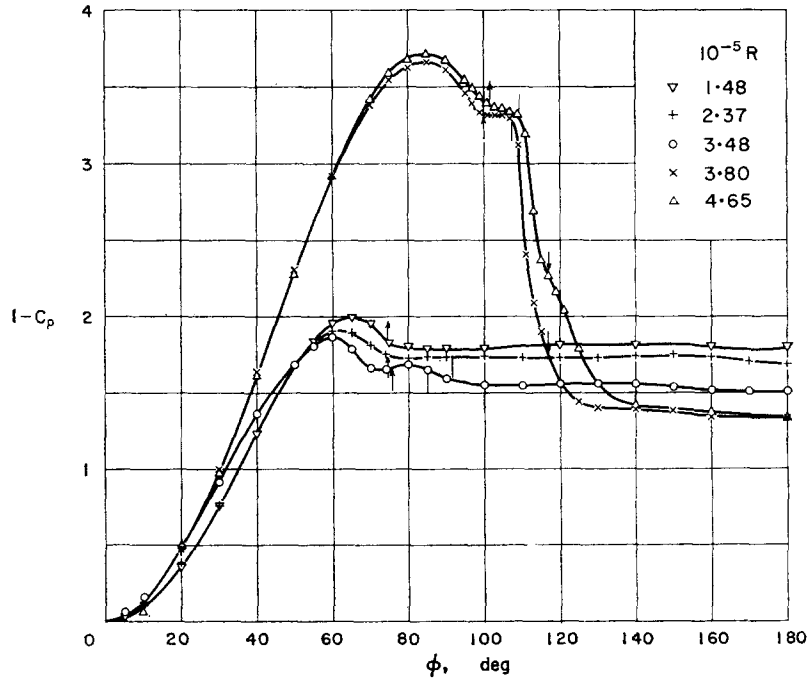

FIG. 12. Pressure distribution on circular cylinder ($d = 16{\cdot}4$ cm). Measurements by Yamamoto and Iuchi[43]. Corrected for tunnel-wall constraint.

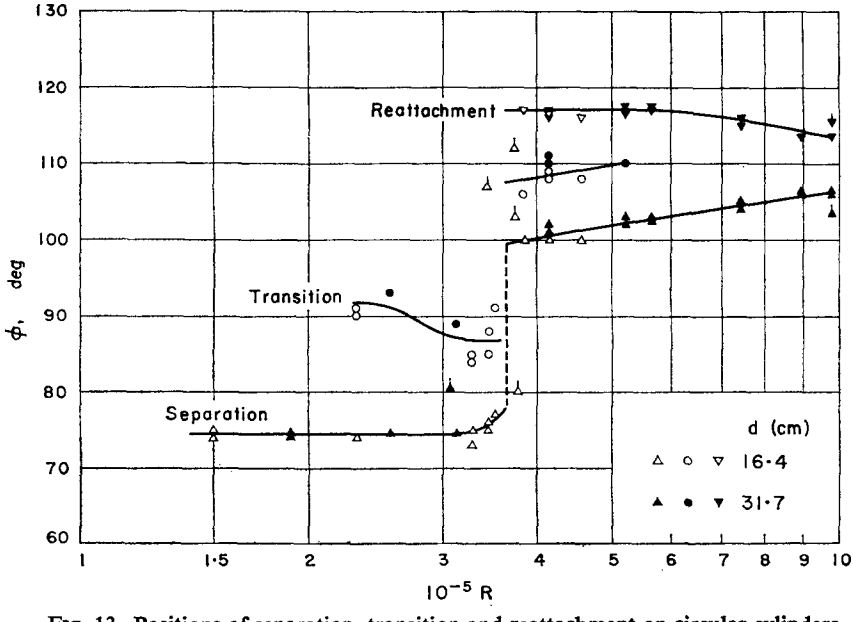

FIG. 13. Positions of separation, transition and reattachment on circular cylinders ($d = 16{\cdot}4$ and $31{\cdot}7$ cm) for Reynolds numbers in the critical range. Measurements by Yamamoto and Iuchi[43].

number. The change from subcritical to supercritical regime takes place usually at a higher Reynolds number than for the change in the reverse direction. Such a hysteresis effect, together with the occurrence of some unstable flow patterns, which were not always repeatable (shown by flagged symbols), is characteristic of most critical changes in type of flow.

A pressure distribution obtained by Roshko[40] at a very high Reynolds number of $8{\cdot}4 \times 10^6$ is shown in Fig. 14. Included for comparison are

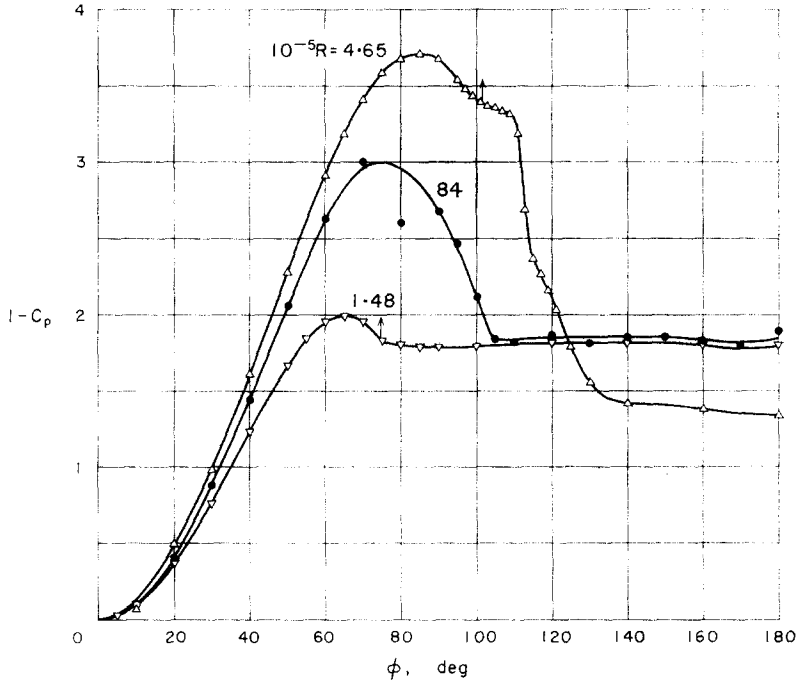

FIG. 14. Pressure distribution on circular cylinder from measurements by Roshko[40] ($R = 8{\cdot}4 \times 10^6$) and by Yamamoto and Iuchi[43] ($R = 1{\cdot}48 \times 10^5$ and $4{\cdot}65 \times 10^5$). Corrected for tunnel-wall constraint.

pressure distributions from Fig. 12, one at a subcritical Reynolds number and the other at a Reynolds number just above the critical transition. Unfortunately, Roshko's experimental points are too widely spaced to be certain of the absence of a bubble, but the indications generally are that laminar separation is precluded by transition in the boundary layer at sufficiently high Reynolds numbers. A similar indication is also shown by the mean curve of pressure distribution obtained by Dryden and Hill[2] from experiments on a smoke stack at a Reynolds number of about 4×10^6.

5. ANALYSIS OF PRESSURE DISTRIBUTION DATA

In the preceding sections, illustrative examples have been presented in the form of surface pressure distributions with the incidence of the aerofoil and the Reynolds number based on aerofoil chord or cylinder diameter as parameters. Since the flow phenomena determining bubble separation are directly related to the behaviour of the boundary layer, it appears appropriate to characterize the flow pattern by a Reynolds number typical of local conditions in the boundary layer. For this purpose the boundary-layer Reynolds number, based on the boundary-layer displacement thickness and the velocity just outside the boundary layer, both measured at separation, appears to be a reasonable choice. Such a quantity as the length of the bubble is then to be related to the displacement thickness at separation.

When a laminar boundary layer separates near the leading edge of an aerofoil, its thickness is so small that, in general, the displacement thickness cannot be determined from measurements of the boundary-layer velocity profile with sufficient accuracy. Moreover, the pressure distribution data reported in the literature are not always accompanied by boundary-layer measurements. For these reasons it is preferable to calculate the displacement thickness from the observed pressure distribution.

The growth of the laminar boundary layer was calculated by the "quadrature formula", which is commonly referred to as Thwaites's formula[20], but in point of fact has been used by Hudimoto[12] and the present author[13] since 1941. This formula is

$$\left(\frac{\theta}{c}\right)^2 R = 0{\cdot}441\left(\frac{U}{U_0}\right)^{-6}\int_0^{s'/c}\left(\frac{U}{U_0}\right)^5 d\left(\frac{s'}{c}\right),$$

in which θ is the momentum thickness of the boundary layer, c is the aerofoil chord, s' is the distance along the surface from the stagnation point, U_0 is the free-stream velocity, U is the velocity just outside the boundary layer, and $R = U_0 c/\nu$ is the free-stream Reynolds number. For application to the flow past a circular cylinder, c was replaced by the cylinder diameter d. The velocity U was related to the pressure coefficient C_p by the equation $U = U_0\sqrt{(1 - C_p)}$. The displacement thickness at separation, δ_s^*, was then calculated from the momentum thickness at separation, θ_s, by assuming 3·7 for the ratio δ_s^*/θ_s, the subscript s denoting conditions at the separation point. Finally, the boundary-layer Reynolds number at separation, $R_{\delta_s}^* = U_s\,\delta_s^*/\nu$, was determined.

Owing to the insufficient accuracy of the theoretical prediction of the laminar separation point, which originates in particular from the need to differentiate an experimental curve, the separation location used in the calculation was that observed by experiment. When no observations of the separation point were reported, as for example, for the pressure distribution

of Fig. 2 for an incidence of 9°, and all the pressure distributions of Fig. 3, the separation was simply assumed to take place at the point where $(1 - C_p)/(1 - C_p)_{max} = 0{\cdot}89$, an average of experimental values pertaining to this type of pressure distribution.

Figure 15 shows the results of the calculation for the NACA 63-009 section, based on the pressure distributions presented in Fig. 2. In addition to the boundary-layer Reynolds number $R^*_{\delta_s}$, the length of the bubble in terms of the displacement thickness l/δ^*_s and the pressure recovery coefficient

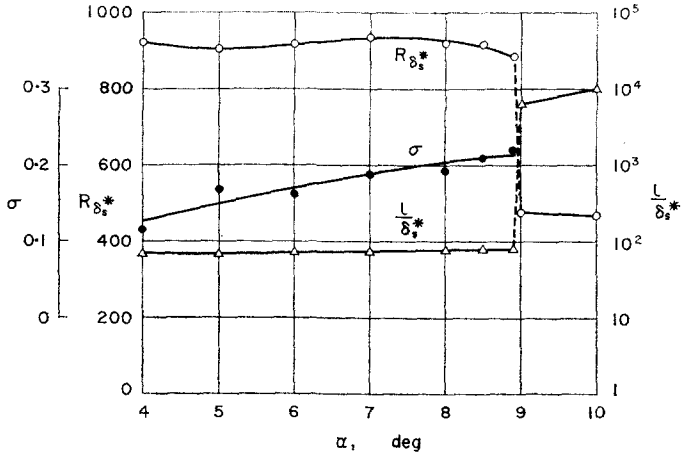

FIG. 15. Calculated boundary-layer Reynolds number at separation, length of bubble and pressure recovery coefficient for NACA 63-009 aerofoil section. $R = 5{\cdot}8 \times 10^6$.

$\sigma = (p_r - p_s)/\frac{1}{2}\varrho\, U_s^2 = (C_{p_r} - C_{p_s})/(1 - C_{p_s})$ are plotted against the incidence α. Here $l = s_r - s_s$ is the distance from separation to reattachment point, and the subscript r denotes conditions at the reattachment point. It is seen that $R^*_{\delta_s}$ maintains a value of about 900 up to an incidence of 8·9°, but suddenly falls to less than 500 at an incidence of 9°, where the short bubble has broken down to form a long bubble. Coincident with this change, l/δ^*_s jumps from a value of order 10^2 to a value of order 10^4. Great accuracy of the results cannot be expected beyond the bubble breakdown, since it was necessary to guess part of the pressure distribution curve near the leading edge in order to calculate δ^*_s. It is believed, nevertheless, that the results are meaningful, and are accurate at least as to order of magnitude. The pressure recovery coefficient σ increases with an increase in incidence, and attains a value of 0·22 before the bubble breaks down.

Figure 16 shows the corresponding results for the NACA 64A006 section, calculated from the pressure distributions given in Figs. 3 and 4. As the short bubble breaks down to form a long bubble at an incidence of 5°,

$R^*_{\delta_s}$ falls from 500 to 400, while l/δ^*_s jumps from 70 to 2100. With further increase in incidence, l/δ^*_s continues to increase until it attains a value of $2{\cdot}5 \times 10^4$ at an incidence of 9°, at which the long bubble extends over the entire chord. The pressure recovery coefficient attains a value of 0·22 before the short bubble breaks down.

The results in Figs. 15 and 16 suggest that representative values of l/δ^*_s for short and long bubbles are 10^2 and 10^4 respectively. Another observation is that $R^*_{\delta_s}$ is less than about 500 when a long bubble is present,

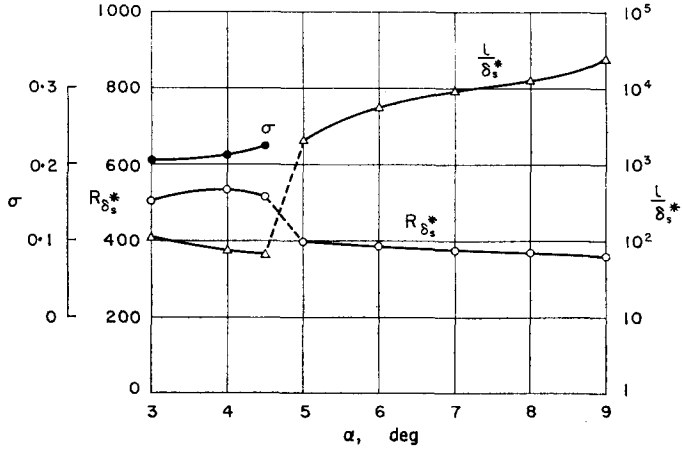

FIG. 16. Calculated boundary-layer Reynolds number at separation, length of bubble and pressure recovery coefficient for NACA 64A006 aerofoil section, $R = 5{\cdot}8 \times 10^6$.

while it is greater than 500 for short bubbles. In order to give more evidence in support of this criterion, additional aerofoil measurements were analysed to produce Table 1, in which values of $R^*_{\delta_s}$ are listed for two incidences—the highest incidence at which a short bubble was observed, and the lowest incidence at which a long bubble was observed. Also included in the table are values of σ at the highest incidence for a short bubble.

The pressure distribution data for the Göttingen 801 section (Fig. 6) are inadequate to permit a detailed analysis, but yield results in rough agreement with those shown in Table 1 in that at a Reynolds number of $4{\cdot}2 \times 10^4$, $R^*_{\delta_s}$ is less than 500, while at a Reynolds number of $7{\cdot}5 \times 10^4$, $R^*_{\delta_s}$ is greater than 500, and l/δ^*_s is of order 10^2.

Figure 17 shows the results of an analysis of the NACA 66_3–018 section at an incidence of 15°, derived from the pressure distribution data of Fig. 9. Stall is imminent at this incidence, especially for the lowest Reynolds number, $1{\cdot}5 \times 10^6$. There the pressure recovery coefficient σ attains a value of 0·34, which is much higher than that found in the preceding data. Further

Table 1. Boundary-layer Reynolds Number at Separation

Aerofoil (NACA)	R	α	$R_{\delta_s^*}$	σ	Type of bubble	Reference
63-009	$5{\cdot}8 \times 10^6$	8·9°	893	0·22	short	18, 22
		9·0°	477		long	
64A006	$5{\cdot}8 \times 10^6$	4·5°	516	0·22	short	19, 22
		5·0°	399		long	
0006	$2{\cdot}7 \times 10^6$	6·0°	520	0.29	short	28
		6·5°	350		long	
	$4{\cdot}6 \times 10^6$	6·5°	671	0·24	short	28
		7·0°	392		long	
	$6{\cdot}8 \times 10^6$	6·0°	774	0·23	short	28
		6·5°	480		long	
0008	$2{\cdot}0 \times 10^6$	8·0°	532	0·27	short	28
		8·5°	352		long	
	$4{\cdot}0 \times 10^6$	9·0°	812	0·24	short	28
		10·0°	426		long	

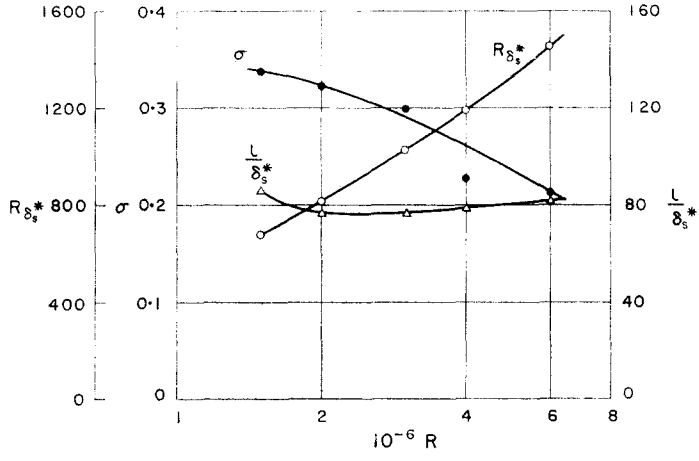

FIG. 17. Calculated boundary-layer Reynolds number at separation, length of bubble and pressure recovery coefficient for NACA 66_3-018 aerofoil section at $\alpha = 15°$.

examples showing a high value of σ prior to bubble breakdown are furnished by Figs. 18 and 19, which are reproduced from Crabtree's analysis[31] of experimental data of McGregor.

Figure 20 shows the results of a calculation on circular cylinders and other bluff bodies, based on the pressure distribution data shown in Figs. 11 and 12, and some additional data on a circular cylinder (Fage[1], Yamamoto and Iuchi[43]), an elliptic cylinder (Schubauer[6, 11]) and a sphere (Fage[7]). The data were analysed to obtain values of $R_{\delta_s}^*$ as functions of the Reynolds

number $R = U_0 d/\nu$, d being the diameter of the circular cylinder or sphere, or the major axis of the elliptic cylinder. The closed symbols denote the points for which the laminar boundary layer separates without subsequent reattachment, while the open symbols denote those for which there is a

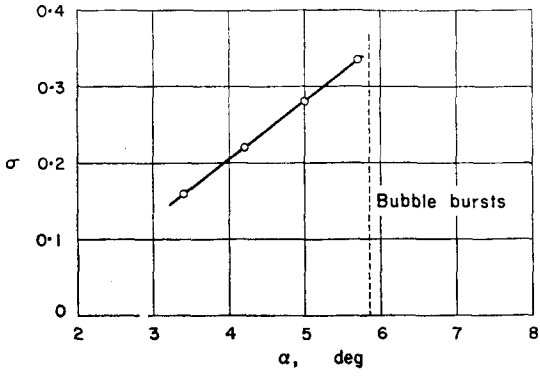

FIG. 18. Variation of pressure recovery coefficient with incidence at $R = 1{\cdot}7 \times 10^6$. Crabtree's analysis[31] of McGregor's experimental data on a Piercy aerofoil.

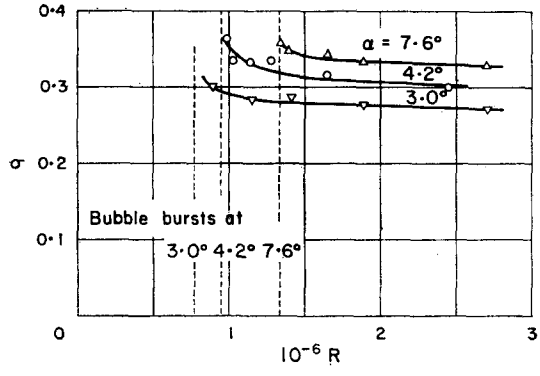

FIG. 19. Variation of pressure recovery coefficient with Reynolds number at constant incidences. Crabtree's analysis[31] of experimental data on McGregor's test model.

laminar separation bubble followed by reattachment as a turbulent boundary layer. In the left half of the figure, which comprises some results from old measurements made in more or less turbulent streams, the regions containing points with closed and open symbols are demarcated by a value of R^*_δ in the neighbourhood of 700. On the other hand, a very distinct demarcation of the points is seen in the right half, which is based on some recent measurements in a less turbulent stream by Yamamoto and Iuchi[43]. The change

from subcritical to supercritical regime takes place at a Reynolds number of $3{\cdot}6 \times 10^5$, and is accompanied by a jump in the value of $R^*_{\delta_s}$ from 950 to 1350. When trip wires of diameter 0·15 mm are placed along generator at $\varphi = \pm 50°$, both the critical Reynolds number and the demarcating value of $R^*_{\delta_s}$ are reduced. Results obtained thus indicate that the critical value of $R^*_{\delta_s}$ decreases with an increase in free-stream turbulence or in surface

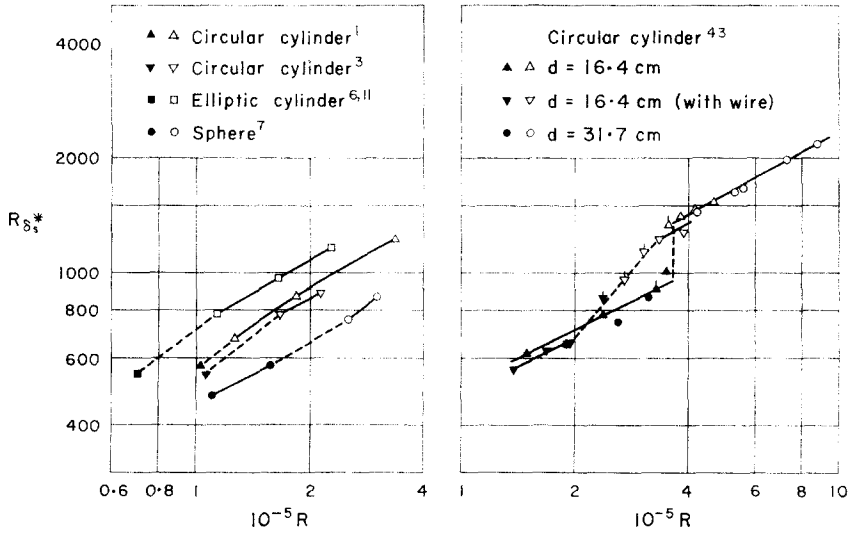

FIG. 20. Calculated boundary-layer Reynolds number at separation on circular cylinder, elliptic cylinder and sphere.

roughness. It will be seen moreover that the critical value is considerably higher than that obtained from experimental data on aerofoils (Table 1).

As mentioned in the preceding sections, there is evidence to show that the laminar separation bubble will not be present beyond a certain value of Reynolds number. For the experimental data on the NACA 66_3-018 aerofoil at an incidence of 2° (Fig. 10), the critical Reynolds number is about 6×10^6, for which the calculated boundary-layer Reynolds number $R^*_{\delta_s}$ is $5{\cdot}5 \times 10^3$ to $5{\cdot}8 \times 10^3$, depending on the assumed location of theoretical laminar separation. The results shown in Fig. 21 provide further evidence in support of this critical value. There l/δ^*_s is plotted against $R^*_{\delta_s}$ for four aerofoil sections at an incidence in the low-drag range. Data for the NACA sections were taken from an analysis made by Bursnall and Loftin,[21] while those for 15 per cent "roof-top" section from a paper by Owen and Klanfer.[23] Downward extrapolation of the curve appears to give a value of 6×10^3 for $R^*_{\delta_s}$ beyond which no bubble will be present. Boundary-layer calculations

were also made on the pressure distribution observed by Roshko at a Reynolds number of $8{\cdot}4 \times 10^6$ (Fig. 14). The value of $R^*_{\delta s}$ was $6{\cdot}2 \times 10^3$ to $6{\cdot}8 \times 10^3$, when separation was assumed to occur at an angular distance of 92–95°. These values are in good agreement with those obtained for aerofoils, but this should be taken with reserve, since Roshko's data on base pressure suggest that the change associated with bubble disappearance takes place

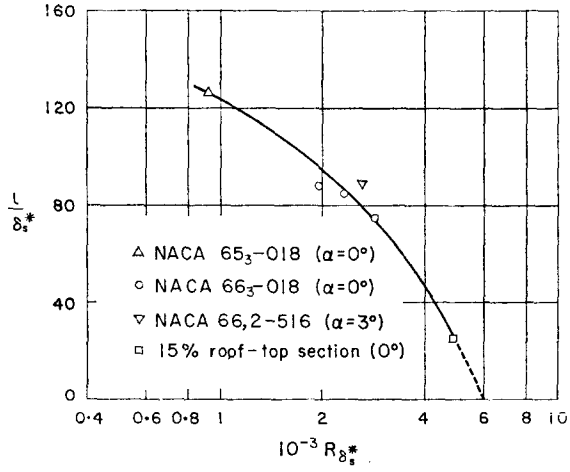

FIG. 21. Variation of bubble length with boundary-layer Reynolds number at separation for aerofoil sections at incidence in the low-drag range.

at a Reynolds number of about $3{\cdot}5 \times 10^6$, for which no pressure distribution data have been reported. If it is assumed that the pressure distribution at this Reynolds number is the same as that at a Reynolds number of $8{\cdot}4 \times 10^6$, the value of $R^*_{\delta s}$ corresponding to bubble disappearance would be reduced to a value in the range $4{\cdot}0 \times 10^3$ to $4{\cdot}4 \times 10^3$.

6. THEORETICAL CONSIDERATIONS

The examples presented in the preceding sections suffice to show that many important characteristics of aerodynamic shapes are intimately associated with the behaviour of the laminar separation bubble. It seems highly desirable, therefore, to develop a theory whereby it is possible to predict the occurrence and extent of separation bubbles in given circumstances. In essence, the criteria required are: one for determining when the separated flow will not reattach to the surface; a second for determining the extent of the bubble if it exists; and a third for determining when the bubble formation will be precluded by transition to turbulence in the boundary layer.

The earliest postulate concerning bubble formation was probably that put forward by von Doenhoff[8,9] on the basis of his experimental observations on the flow along a flat plate with an adverse pressure gradient.

Von Doenhoff speculated that the separated flow proceeds along the direction of the tangent to the surface at the separation point, and that transition to turbulence takes place in the separated flow, whereupon the subsequent turbulent *entrainment* causes the flow to return to the surface. He assumed that the length of separated laminar flow is determined by a constant value of the Reynolds number based on the velocity U_s outside of the boundary layer at separation and the distance l_1 between the points of separation and transition. He suggested a value of 5×10^4 for this Reynolds number $U_s l_1/\nu$ and a value of 15° for the deflection angle of the inner boundary of the separated flow. The bubble is then represented by a flat triangular region sketched in Fig. 22, and the condition under which flow reattachment will

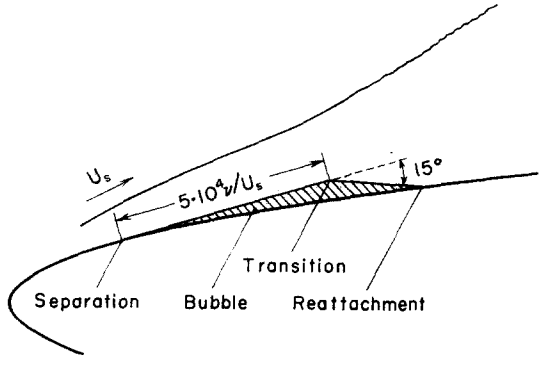

FIG. 22. Von Doenhoff's concept of bubble formation.

not take place is determined graphically. This simple concept has proved most helpful in explaining qualitatively many of the effects of Reynolds number on the stalling characteristics of aerofoil sections.

The interpretation that the onset of turbulence in the separated flow is responsible for the reattachment appears extremely plausible. An indication of its validity has been obtained from the results of subsequent measurements,[21,27] wherein fully developed turbulence is first observed in the separated flow fairly close to that position where the flow begins to return to the surface and the corresponding pressure recovery occurs.† Nevertheless, the schematic representation of a bubble shown in Fig. 22 appears to oversimplify the process of reattachment. By analysis of the experimental results on a bubble near the leading edge of the NACA 63-009, 66_3-018 and modified 0010 aerofoil sections, Gault[27] found values of the deflection angle ranging from 6° to 52°, and of the Reynolds number $U_s l_1/\nu$ from 4×10^4 to 8×10^4. An increase in the intensity of free-stream turbulence to 1·1 per cent reduced the value of $U_s l_1/\nu$ to 3×10^4. Thus, neither the invariance of the Reynolds number, nor the existence of a unique value of deflection angle seems

† This position can be most clearly located in the pressure distribution curve of Fig. 9 by the abrupt rise in pressure, amounting practically to a break in the curve.

to be correct. Seeing that the observed values lie within a rather limited range, however, the physical concept may be not very far from the truth.

Experimental evidence of the failure of flow reattachment at sufficiently low Reynolds numbers led the present author[10] to seek a criterion for the occurrence of reattachment. He postulated from dimensional considerations that the boundary-layer Reynolds number at separation must exceed a certain critical value if the separated flow is to reattach to the surface. He suggested a value of 210 for the Reynolds number $U_s \theta_s/\nu$ based on the momentum thickness θ_s after analysing the small number of available experimental data on circular[1, 3] and elliptic cylinders,[6, 11] and spheres.[7] If a value of 3·7 is assumed for the ratio δ_s^*/θ_s, the critical value of the Reynolds number based on the displacement thickness $R_{\delta_s}^*$ becomes 780, which is a little higher than the value obtained from the left half of Fig. 20. The discrepancy is attributed to the inaccuracy of the method of analysis. Another point which was not correct was the assumption that the critical value would be the same for a bubble near the leading edge of an aerofoil and could be used to explain quantitatively the effect of Reynolds number on its stalling characteristics. As seen from the results in Table 1, the critical value of $R_{\delta_s}^*$ is about 500 for aerofoils, at least in the case where the bubble is formed near the leading edge.

Maekawa and Atsumi[16] carried out measurements on the region of separated flow downstream of the intersection of two plane surfaces and observed that the reverse flow forms a circulating motion which attracts the separated flow toward the surface. Flow reattachment will not occur unless sufficient energy is supplied to maintain the circulating motion against dissipation. On the basis of this reasoning Maekawa and Atsumi suggested that the Reynolds number based on the total extent of separated flow must be less than a certain critical value. They also suggested that the boundary-layer Reynolds number at separation must be greater than a certain critical value for the separated flow to become sufficiently unstable for the circulating motion to be energized. The latter condition is the same as the criterion proposed by Tani.[10] However, considerable doubt has been expressed[31] as to whether the flow separation occurring at the intersection of two plane surfaces is exactly equivalent to that which produces a short bubble on the aerofoil surface. For this reason the results of Maekawa and Atsumi's measurements have not been used in the present analysis, although the physical concept involved appears to be correct.

Later, Owen and Klanfer[23] independently put forward a similar criterion in terms of $R_{\delta_s}^*$ on the basis of their analysis of available experimental data on bubbles on aerofoils and in regions of interaction between a shock wave and a boundary layer. They found that the bubble is short or long according to whether $R_{\delta_s}^*$ is greater or less than a critical value in the neighbourhood of 400–500. This critierion is confirmed by the results shown in Table 1, which contains only data on bubbles near the leading edge of an aerofoil.

The criterion successfully distinguishes between short and long bubbles of separated flow, but as pointed out by Gault,[27] there appears to be no universal critical value of $R^*_{\delta_s}$ for the breakdown of a short bubble. As soon as a short bubble has broken down, the value of $R^*_{\delta_s}$ falls to less than about 500, although immediately prior to breakdown $R^*_{\delta_s}$ may be appreciably greater than 500 (Fig. 15 and Table 1). This is not altogether surprising, since the breakdown brings about a radical readjustment of the pressure distribution. From this argument it is clear that the criterion based on $R^*_{\delta_s}$ is not the condition for the breakdown of a short bubble. It is meant only as a statement that $R^*_{\delta_s}$ is always greater than about 500 whenever a short bubble is present. In this sense it is essentially the same as the criterion advanced by Tani,[10] although Tani's suggested value of $R^*_{\delta_s}$ is appropriate for the flow about bluff bodies.

The significance of the boundary-layer Reynolds number in this criterion is now obvious: at high Reynolds numbers an instability develops in the separated flow. It eventually produces turbulence, which is considered to be a prerequisite for flow reattachment to the surface. This view appears to be supported by the experimental evidence that the critical value of $R^*_{\delta_s}$ is reduced with an increase in free-stream turbulence or in surface roughness. As another possible explanation, Crabtree[31] mentioned Schubauer and Klebanoff's experimental observation that turbulent spots grow rapidly in the boundary layer on a flat plate when the Reynolds number based on displacement thickness is greater than about 450. However, the situation may be different for a separated layer away from the surface, and the coincidence of values of boundary-layer Reynolds number seems to be only fortuitous.

Contrary to the previous expectation of the present author,[10] it has turned out that the critical value of $R^*_{\delta_s}$ depends upon whether the bubble is formed on circular cylinders or near the leading edge of aerofoils. If the differences in pressure gradient and in surface curvature in the two cases are considered, the difference in behaviour of the separated flows is perhaps not too difficult to understand. Further research is needed, however, in order to give a full explanation for the difference in critical value of $R^*_{\delta_s}$. It would also be interesting to examine the critical value of $R^*_{\delta_s}$ for the bubble formed behind the position of maximum suction on an aerofoil at incidences within the low-drag range. No measurements have been reported.

It is perhaps appropriate at this stage to mention the boundary-layer calculations carried out by Curle and Skan[36] based upon the theoretical inviscid pressure distributions for the RAE family of aerofoil sections. The results of their calculations are reproduced in Fig. 23, in which the value of $k = R^*_{\delta_s}/\sqrt{R}$ is plotted against the lift coefficient C_L for four aerofoil sections. It is seen that k drops fairly sharply to a minimum as C_L increases, and then increases very slowly with further increase in C_L. This minimum value of k has led Curle and Skan to provide a possible explanation of bubble breakdown: as C_L increases beyond the critical value, laminar separation will take

place. If the value of k is large enough, the separation bubble will be short because $R^*_{\delta_s}$ will become greater than 500. As C_L increases, however, k decreases, and if it decreases sufficiently, the short bubble may burst. This would appear most likely to occur when k has reached the minimum value, and if it has not occurred then, a further increase in C_L should not cause the bubble to burst.

Curle and Skan's theoretical analysis may be of use for giving information about the lift coefficient or the incidence at which a short bubble breaks

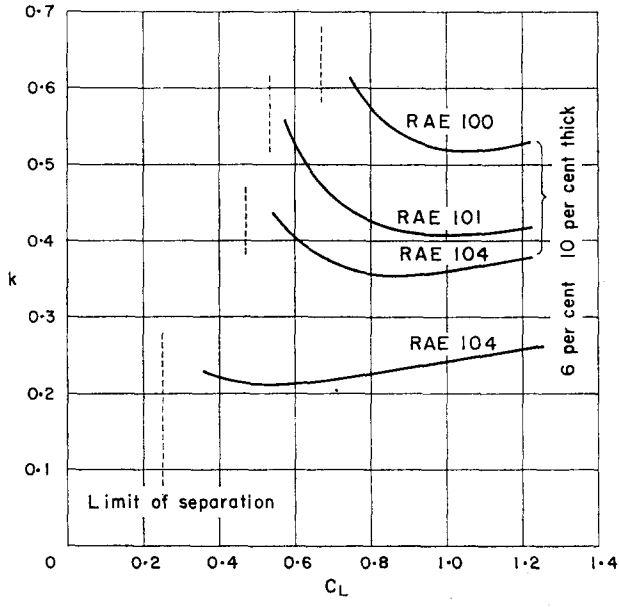

FIG. 23. Variation of ratio $R^*_{\delta_s}/\gamma R$ with lift coefficient for four RAE aerofoil sections. Calculation by Curle and Skan[36].

down to form a long bubble on the aerofoil. But, because the theory is based on the criterion of Tani[10] and Owen and Klanfer,[23] it does not furnish any new condition for the breakdown of a short bubble.

Wallis[24, 42] and his co-workers carried out experimental observations on aerofoil models provided with either air jets or roughness strips for the purpose of simulating high Reynolds number flows, and found that the reattached turbulent boundary layer exhibits just downstream of the reattachment point a peak in the development of the shape parameter H, the ratio of displacement and momentum thicknesses. As incidence is increased, the peak value of H increases and approaches the value associated with turbulent separation. With the model smooth and the air jet off, the variation of H was found to be almost constant. Wallis then made the suggestion that the separation, or more correctly, *reseparation* of the reattached turbulent

boundary layer provides the mechanism of flow breakdown, at least for moderate to high Reynolds numbers. On the other hand, however, Wallis postulated that the flow pattern involving a short bubble, a short extent of attached turbulent boundary layer, and subsequent complete separation, is not stable, so that the flow leaves at the laminar separation point to form a long bubble.

Further evidence of turbulent reseparation was presented by Moore[35] from his measurements on a raised-nose aerofoil model provided with an

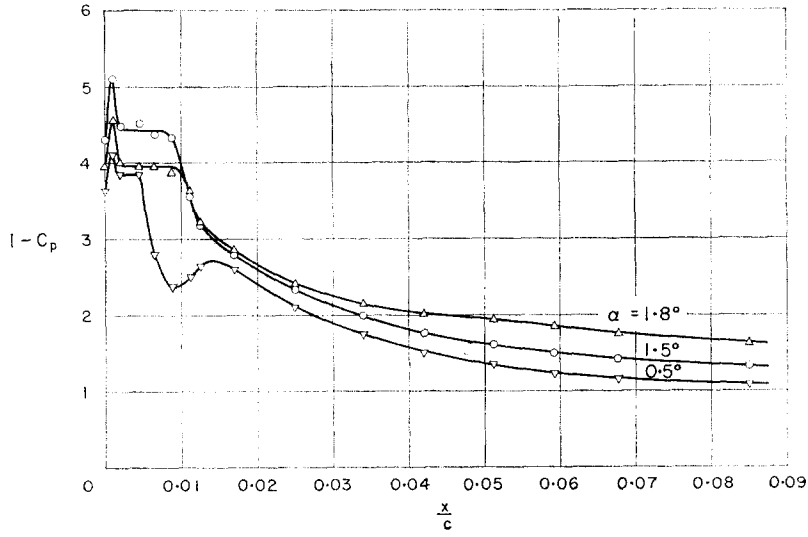

FIG. 24. Pressure distribution on a raised-nose aerofoil model provided with an auxiliary aerofoil. $R = 1{\cdot}8 \times 10^6$. Measurements by Moore[35].

auxiliary aerofoil. Pressure distributions near the leading edge of the model are shown in Fig. 24. They indicate constant pressure and pressure recovery regions, revealing the presence of a short bubble.† Contrary to the examples shown in Sections 2 and 3, an increase in incidence causes the bubble to expand in the downstream direction until breakdown occurs to form a long bubble at an incidence just beyond 1·8°. The corresponding boundary-layer behaviour is shown in Fig. 25, in which values of H are plotted against the distance from the leading edge. There are fairly good indications that turbulent separation starts near $x/c = 0{\cdot}08$, and that with increasing incidence it moves rapidly forward toward the downstream edge of the bubble.

However, there is some doubt as to whether the flow obtained by this particular arrangement is exactly equivalent to that which produces a short

† The kink of the pressure distribution curve downstream of the bubble at an incidence of 0·5° is probably due to the influence of the auxiliary aerofoil.

bubble near the leading edge of a thin aerofoil. It should be mentioned in this connection that no region of incipient turbulent separation was detected by McCullough and Gault[18, 22] just downstream of a short bubble on the NACA 63-009 aerofoil (Fig. 2).

In the experimental results discussed by Wallis and Moore, the reattached turbulent boundary layer exhibits a peak in the development of H, the peak value increasing with increasing incidence. Upon closer examination, it is found that the increase in the peak value of H is mostly accounted for by the

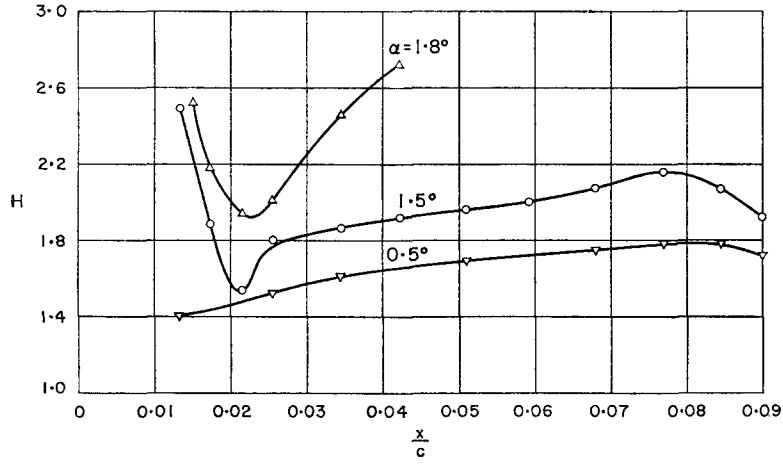

FIG. 25. Distribution of shape parameter H on the same aerofoil model as in Fig. 24. $R = 1{\cdot}8 \times 10^6$. Measurements by Moore[35].

increase in the initial value of H, namely the value at the reattachment point. The latter value increases as the reattachment becomes less complete. This reasoning leads one to conclude that when the flow breakdown is caused by a reseparation just downstream of reattachment, this amounts to the same thing as the bubble breakdown itself.

Evans and Mort[34] put forward an analysis from which it is inferred that there are two distinct mechanisms of abrupt stall. One is presumed to be due to the breakdown of the bubble, and the other due to the reseparation of the turbulent boundary layer. The data which were analysed were not those experimental results in which the pressure distribution was measured, but rather the standard force test data on two-dimensional aerofoil models in the NACA low-turbulence pressure tunnel at a Reynolds number of 6×10^6. The only data used were those for which the stall is abrupt, as selected according to the requirement that the two points of the lift curve which bound the stall should indicate a slope $\Delta C_L/\Delta\alpha$ of at least 0·1 per degree, with ΔC_L itself at least 0·1. From the theoretical velocity distribution for inviscid

flow just prior to the stall, a boundary-layer calculation was made to obtain the value of the boundary-layer Reynolds number at separation, $R^*_{\delta_s}$, the separation being assumed to occur where the velocity has fallen 6 per cent from its peak value, U_{max}. For each velocity distribution, the distance to the separation point, Δs_l, as shown in the inset of Fig. 26, was employed as a measure of the adverse pressure gradient. By plotting the peak velocity ratio U_{max}/U_0 against the adverse distance ratio $\Delta s_l/c$, as reproduced in Fig. 26, Evans and Mort observed that a good correlation exists for those points for which $R^*_{\delta_s}$ is greater than about 1300. A correlation between high peak

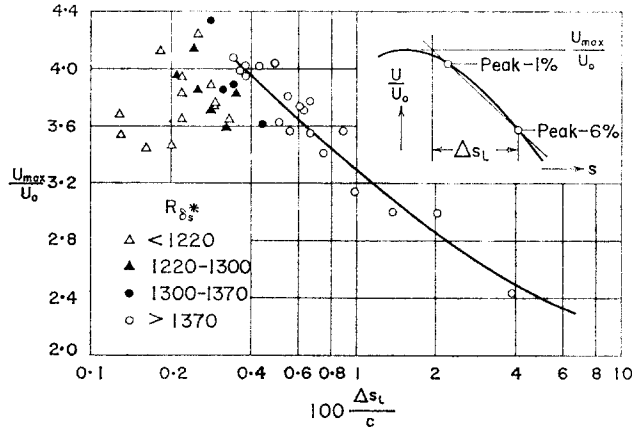

FIG. 26. Correlation of peak velocity at abrupt stall with adverse distance. Analysis by Evans and Mort[34].

velocity and short adverse distance is to be expected from the assumption of stall ascribed to the reseparation mechanism, but not from that ascribed to the bubble breakdown mechanism. This argument led Evans and Mort to adopt the view that there is a critical value of $R^*_{\delta_s}$ above which abrupt stalls are due to reseparation, and below which they are due to bubble breakdown.

In seeking a criterion for bubble breakdown, Crabtree[25] made the plausible assumption that the breakdown occurs because there exists a maximum possible value of pressure that can be recovered in the turbulent entrainment process causing the flow reattachment. He then indicated[31] by analysis of the available experimental results that the value of the pressure recovery coefficient σ gradually increases with either an increase in incidence at constant Reynolds number (for example, see Fig. 18), or with a decrease in Reynolds number at constant incidence (for example, see Figs. 17 and 19). He concluded that when σ attains a value of about 0·35, the bubble suddenly breaks down to give rise to a flow pattern associated with a long bubble.

In further corroboration of the existence of a maximum pressure recovery, Norbury and Crabtree[26, 32] made an analysis of the simplified bubble

flow model which is depicted in Fig. 27. They assumed that the turbulent entrainment process and the corresponding pressure recovery occur only in the region ABRT, that the fluid passing through AT is diffused to form a boundary layer of thickness BR in such a way that the velocity along the streamline AB falls from U_t to U_r without loss of energy, that neither fluid mass nor momentum enters or leaves the region across TV on the average, that the shear stress acting on the surface VR is negligibly small, and that the curvature of the surface SVR is negligible and AB is parallel to VR. They made the further assumptions that the velocity profile across AT is given by $u = U_t\{a + (1 - a)(y/\delta_t)\}$, where $\delta_t = \overline{AT}$, and that the profile across BR is given by $u = U_r(y/\delta_r)^n$, where $\delta_r = \overline{BR}$. Application of the equation

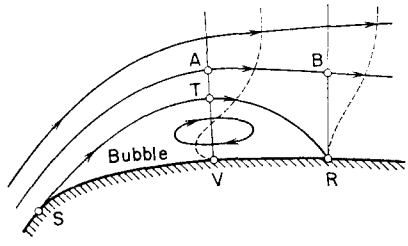

FIG. 27. Norbury and Crabtree's simplified model of flow pattern with a bubble.

of continuity and the momentum theorem to the region ABRV yields an expression for the pressure recovery coefficient σ, which in this simplified model is given by $(p_r - p_t)/\frac{1}{2}\varrho\, U_t^2$, where p_t and p_r are the pressure in the sections ATV and BR, respectively. The variation of pressure in the direction normal to the surface is neglected. In the limiting case $n = 1$, Norbury and Crabtree obtained values of σ varying from 0·37 to 0·45 as the constant a was varied from 1 to 0·5, although it appears that the value of σ for $a = 0{\cdot}5$ is wrong and should have been corrected to 0·15.

Further experimental confirmation was presented by Moore[35], who suggested 0·36 for the maximum value of σ. There are other experimental results, however, in which σ also increases with the increase in incidence, but attains a maximum of only 0·22 before the bubble breaks down. See, for example, Figs. 15 and 16, and also Table 1. It appears therefore that a value of 0·35 should be considered as an upper limit. It remains unknown what parameters control the value of σ just prior to bubble breakdown.

Nevertheless, the existence of a maximum pressure recovery might possibly be corroborated by realizing that the bubble is maintained by the turbulent shear stress set up in the entrainment region.[41] For simplicity it is assumed that the pressure is constant and equal to p_s from the separation point S to the bubble top T and then rises linearly with distance to attain a value p_r at the reattachment point R (see Fig. 28), the variation of pressure

across the bubble being neglected.† Then the resultant of the pressure acting on the boundary STR is $\frac{1}{2}h(p_r - p_s)$, directed to the left, where $h = \overline{TV}$. Transition is assumed to take place in the neighbourhood of T, so that the resultant of shear stress acting on the boundary TR amounts to $l_2\tau$, directed to the right, where $l_2 = \overline{VR}$ and τ denotes the shear stress averaged over the boundary TR. Equilibrium of forces requires

$$-\tfrac{1}{2}h(p_r - p_s) + l_2\tau = 0,$$

whence the pressure recovery coefficient is

$$\sigma = \frac{2l_2}{h}\frac{\tau}{\frac{1}{2}\varrho\, U_s^2}.$$

Examination of experimental results presented in References 14, 21, 22, 27 and 31 gives a value ranging from 15 to 40 for $2l_2/h$. There exists no experimental data for the shear stress acting on the bubble on an aerofoil

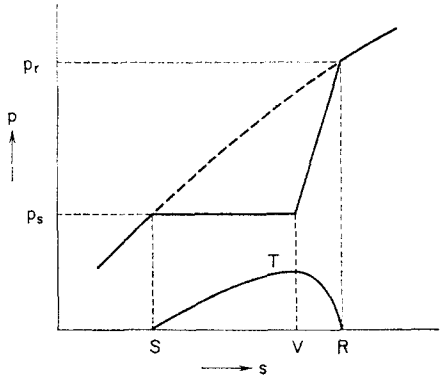

FIG. 28. Simplified pressure distribution on separation bubble.

model, but useful information may be obtained from the measurements on a half jet[15] and a separated flow over a step or a groove.[33, 39] The maximum value of $\tau/\frac{1}{2}\varrho\, U_s^2$ observed in these measurements ranges from 0·01 to 0·02. Multiplication of the two values gives a value ranging from 0·15 to 0·80 for σ, which is of the same order of magnitude as the maximum possible value 0·35. It seems therefore that the existence of a maximum pressure recovery is accounted for by the existence of a maximum possible shear stress in the turbulent entrainment.

Another corroboration[37, 41] may be provided by making use of the postulate put forward by Korst[29] and Chapman, Kuehn and Larson[30] for the analysis of base pressure phenomena at high speeds. The postulate amounts to assuming no loss in total pressure along the boundary stream-

† In this simplified model, the velocity U_t outside of the boundary layer at the point T is equal to the outside velocity at separation, U_s.

line TR, and leads to the relation

$$p_s + \tfrac{1}{2}\varrho\, a^2\, U_s^2 = p_r,$$

where $a\, U_s$ is the velocity at the point T. The pressure recovery coefficient is then given by

$$\sigma = a^2.$$

Determination of the value of a is made by considering the constant-pressure laminar entrainment process along the boundary streamline ST. If the boundary-layer thickness at separation is zero, Chapman's calculation[17] applies directly and gives a constant value of 0·587 for the velocity ratio a, that is, the ratio of the velocity on the boundary streamline to that at the outside of the entrainment region. If the boundary-layer thickness at separation is sizable, the velocity ratio a is zero at the outset, and increases with the distance from separation, approaching asymptotically to a constant value of 0·587. The approach becomes more gradual as the boundary-layer thickness is increased. In view of these circumstances, the value of σ obtained by taking $a = 0{\cdot}587$, that is, $\sigma = 0{\cdot}587^2 = 0{\cdot}345$, may be considered to be an upper limit. Further, as the incidence is increased, the laminar separation point moves forward so that the boundary-layer thickness at separation is reduced. This accounts for the increase in pressure recovery coefficient with incidence as observed in the preceding examples.

7. CONCLUSION

The foregoing arguments have led the author to take the following views on the mechanism of bubble separations.

The bubble is formed by the separation of a laminar boundary layer with a subsequent reattachment, which is believed to be accomplished by the entrainment process of the turbulence initiated in the separated flow. An analysis of the available experimental data suggests that the bubble formation is possible only when the Reynolds number based on boundary-layer displacement thickness at separation is greater than a certain critical value (Tani, Owen and Klanfer criterion). The analysis further indicates that the pressure recovery coefficient (pressure recovered in the reattachment process in terms of the dynamic pressure at separation) can only be less than a certain critical value (Crabtree criterion). The situation just prior to the breakdown of a bubble, caused by either an increase in incidence or a decrease in Reynolds number, is that the first criterion is fulfilled and that the second criterion is about to be violated. The first criterion may be interpreted as an assurance that transition to turbulence will occur in the separated flow. The second criterion implies the existence of a maximum possible value of the shear stress set up in the turbulent entrainment region so as to counteract the pressure gradient. It appears that the critical values pertinent to these criteria are not necessarily universal. For example, the critical boundary-layer Reynolds number at separation is different in the two cases where the bubble is formed on a

circular cylinder and near the leading edge of an aerofoil. Also the maximum value of the pressure recovery coefficient attained just prior to a bubble breakdown is not always the same. It remains unknown as to what causes the difference in the critical values. Further research is needed in order to give full explanation to these problems.

REFERENCES

1. FAGE, A. The airflow around a circular cylinder in the region where the boundary layer separates from the surface. A.R.C. R. & M. 1179 (August 1928).
2. DRYDEN, H. L. and G. C. HILL. Wind pressure on circular cylinders and chimneys. *Bur. Stand. J. Res., Wash.* **5**, 653–693 (Sept. 1930).
3. FAGE, A. and V. M. FALKNER. Further experiments on the flow around a circular cylinder. A.R.C. R. & M. 1369 (Feb. 1931).
4. JONES, B. M. An experimental study of the stalling of wings. A.R.C. R. & M. 1588 (Dec. 1933).
5. JONES, B. M. Stalling. *J. R. Aero. Soc.* **38**, 753–770 (Sept. 1934).
6. SCHUBAUER, G. B. Air flow in a separating laminar boundary layer. NACA TR 527 (1935).
7. FAGE, A. Experiments on a sphere at critical Reynolds numbers. A.R.C. R. & M. 1766 (Sept. 1936).
8. VON DOENHOFF, A. E. A preliminary investigation of boundary-layer transition along a flat plate with adverse pressure gradient. NACA TN 639 (March 1938).
9. JACOBS, E. N. and A. E. VON DOENHOFF. Transition as it occurs associated with and following laminar separation. *Proc. Fifth Int. Congr. Appl. Mech.*, September 1938, 311–314, Wiley, 1939.
10. TANI, I. Note on the interplay between the laminar separation and the transition from laminar to turbulent of the boundary layer (in Japanese). *J. Soc. Aero. Sci. Japan* **6**. 122–134 (Feb. 1939).
11. SCHUBAUER, G. B. Air flow in the boundary layer of an elliptic cylinder. NACA TR 652 (1939).
12. HUDIMOTO, B. An approximate method for calculating the laminar boundary layer (in Japanese). *J. Soc. Aero. Sci. Japan* **8**, 279–282 (March 1941).
13. TANI, I. A simple method for determining the laminar separation point (in Japanese). *J. Aero. Res. Inst. Univ. Tokyo*, **199**, 62–67 (March 1941).
14. VON DOENHOFF, A. E. and N. TETERVIN. Investigation of the variation of lift coefficient with Reynolds number at a moderate angle of attack on a low-drag airfoil. NACA Wartime Rep. L-661 (Nov. 1942).
15. LIEPMANN, H. W. and J. LAUFER. Investigations of free turbulent mixing. NACA TN 1257 (August 1947).
16. MAEKAWA, T. and S. ATSUMI. Transition caused by the laminar flow separation (in Japanese). *J. Soc. Appl. Mech. Japan* **1**, 187–192 (Nov. 1948). Translated as NACA TM 1352 (1952).
17. CHAPMAN, D. R. Laminar mixing of a compressible fluid. NACA TN 1800 (Feb. 1949); superseded by NACA TR 958 (1950).
18. GAULT, D. E. Boundary-layer and stalling characteristics of the NACA 63-009 airfoil section. NACA TN 1894 (June 1949).
19. MCCULLOUGH, G. B. and D. E. GAULT. Boundary-layer and stalling characteristics of the NACA 64A006 airfoil section. NACA TN 1923 (August 1949).
20. THWAITES, B. Approximate calculation of the laminar boundary layer. *Aero. Quart.* **1**, 245–280 (Nov. 1949).
21. BURSNALL, W. J. and L. K. LOFTIN, Jr. Experimental investigation of localized regions of laminar-boundary-layer separation. NACA TN 2338 (April 1951).

22. McCULLOUGH, G. B. and D. E. GAULT. Examples of three representative types of airfoil-section stall at low speed. NACA TN 2502 (Sept. 1951).
23. OWEN, P. R. and L. KLANFER. On the laminar boundary layer separation from the leading edge of a thin aerofoil. RAE Rep. Aero. 2508 (Oct. 1953); reissued as A.R.C. CP 220 (1955).
24. WALLIS, R. A. Experiments with air jets to control the nose stall on a 3 ft. chord NACA 64A006 aerofoil. Aero. Res. Lab. (Australia), Aero. Note 139 (Sept. 1954).
25. CRABTREE, L. F. The formation of regions of separated flow on wing surfaces. Part I. Low-speed tests on a two-dimensional unswept wing with a 10 per cent thick RAE 101 section. RAE Rep. Aero. 2528 (Nov. 1954); reissued as Part I of A.R.C. R. & M. 3122 (1959).
26. NORBURY, J. F. and L. F. CRABTREE. A simplified model of the incompressible flow past two-dimensional aerofoils with a long bubble type of flow separation. RAE Rep. Aero. 2352 (June 1955).
27. GAULT, D. E. An experimental investigation of regions of separated laminar flow. NACA TN 3505 (Sept. 1955).
28. McCULLOUGH, G. B. The effect of Reynolds number on the stalling characteristics and pressure distributions of four moderately thin airfoil sections. NACA TN 3524 (Nov. 1955).
29. KORST, H. H. A theory for base pressures in transonic and supersonic flow. *J. Appl. Mech.* **23**, 593–600 (Dec. 1956).
30. CHAPMAN, D. R., D. M. KUEHN and H. K. LARSON. Investigation of separated flows in supersonic and subsonic streams with emphasis on the effect of transition. NACA TN 3869 (March 1957).
31. CRABTREE, L. F. The formation of regions of separated flow on wing surfaces. Part II. Laminar-separation bubbles and the mechanism of the leading-edge stall. RAE Rep. Aero. 2578 (July 1957); reissued as Part II of A.R.C. R. & M. 3122 (1959).
32. CRABTREE, L. F. Effects of leading-edge separation on thin wings in two-dimensional incompressible flow. *J. Aero. Sci.* **24**, 597–604 (August 1957).
33. TANI, I. Experimental investigation of flow separation over a step. *Grenzschicht-forschung, Symposium Freiburg i. Br.*, August 1957, 377–386, Springer-Verlag, 1958.
34. EVANS, W. T. and K. W. MORT. Analysis of computed flow parameters for a set of sudden stalls in low-speed two-dimensional flow. NASA TN D-85 (August 1959).
35. MOORE, T. W. F. A note on the causes of thin aerofoil stall. *J. R. Aero. Soc.* **63**, 724–730 (Dec. 1959).
36. CURLE, N. and S. W. SKAN. Calculated leading-edge laminar separations from some RAE aerofoils. A.R.C. CP 504 (1960).
37. SAVAGE, S. B. An approximate analysis for reattaching turbulent shear layers in two-dimensional incompressible flow. Mech. Engng. Res. Lab., McGill Univ., Montreal, Rep. Ae 3 (Sept. 1960).
38. KRAEMER, K. Flügelprofile im kritischen Reynoldszahl-Bereich. *Forsch. a. d. Geb. d. Ing.* **27**, 33–46 (1961).
39. TANI, I., M. IUCHI and H. KOMODA. Experimental investigation of flow separation associated with a step or a groove. Rep. Aero. Res. Inst., Univ. Tokyo, 364 (April 1961).
40. ROSHKO, A. Experiments on the flow past a circular cylinder at very high Reynolds number. *J. Fluid Mech.* **10**, 345–356 (May 1961).
41. TANI, I. Critical survey of published theories on the mechanism of leading-edge stall. Rep. Aero. Res. Inst., Univ. Tokyo, 367 (June 1961).
42. WALLIS, R. A. Boundary layer transition at the leading edge of thin wings and its effect on general nose separation. *Advances in Aeronautical Sciences* **3**, 161–184, Pergamon Press, 1962.
43. YAMAMOTO, K. and M. IUCHI. to be published.